Progress of Theoretical Physics, Vol. 48, No. 5, November 1972

Energy Gap in Neutron-Star Matter*)

Tatsuyuki TAKATSUKA

Department of Nuclear Engineering, Kyoto University, Kyoto

(Received April 24, 1972)

On exactly taking into account the attractive effect of the ${}^3P_2-{}^3F_2$ coupling due to the two-nucleon tensor force and the effect of the one-body potential, the density region in the neutron-star matter where the ${}^3P_2$-superfluid state exists is determined as $\rho \simeq (2\sim 8)\times 10^{14}\mathrm{gcm}^{-3}$. The tensor coupling effect is shown to play an indispensable role on the existence of the ${}^3P_2$-gap in neutron-star matter. The ${}^1S_0$-gap is also investigated, leading to the result that the ${}^1S_0$-superfluid state exists in the density region $\rho \simeq (1.0\times 10^{11}\sim 1.5\times 10^{14})\mathrm{gcm}^{-3}$. On the basis of these results, the region $\rho \simeq (1.5\sim 2.0)\times 10^{14}\mathrm{gcm}^{-3}$ is considered to result in the normal state.

§ 1. Introduction

In a series of papers I$\sim$III[1)~3)] we have investigated the existence of the neutron superfluidity originating from the ${}^3P_2$-pairing in a high-density region of the neutron-star matter. Its presence has been pointed out in I[2)] and demonstrated in II[3)] by solving the coupled integral equations for all the types of the ${}^3P_2$-gap by using the existing several semiphenomenological two-nucleon potentials. The boundaries in the density for its existence have not yet been sharply determined, although we have concluded that it appears at least for $\rho \simeq (2\sim 5)\times 10^{14}\mathrm{gcm}^{-3}$.

In a low-density region of neutron-star matter, $\rho \lesssim 1\times 10^{14}\mathrm{gcm}^{-3}$, the superfluidity is well known to exist in the ${}^1S_0$ state. The ${}^1S_0$-gap in neutron-star matter has been particularly investigated by several authors,[4),5)] but the boundaries for its existence in neutron-star matter remain undetermined, too.

It has also been remarked in II that the intermediate-density region, $\rho \simeq (1\sim 2)\times 10^{14}\mathrm{gcm}^{-3}$ where both the ${}^1S_0$- and ${}^3P_2$-gaps are considered to be zero or vanishingly small, should be more carefully investigated. Whether this region corresponds to the normal or superfluid state will be connected with the properties of a neutron star (thermal, rotational, magnetic and so on), because it is in the typical densities of neutron-star matter. As for the ${}^1D_2$-pairing, it has been concluded in II that the energy gap due to this pairing does not take place. Therefore, our investigation of this intermediate region may be safely restricted to the ${}^1S_0$- and ${}^3P_2$-pairings.

In this paper we intend to determine more reliably the density region where the ${}^3P_2$-superfluid state exists. We also determine the density region where the ${}^1S_0$-superfluid state is present. Based on these studies, we aim to investigate

*) A preliminary report on a part of this paper has been published in Ref. 1).

whether the intermediate region in question yields the normal or superfluid state. We pay attention especially to the following two points:

(1) Generally, every gap in the matter of nucleons is very sensitive to the effective mass, M^*, of a nucleon. Therefore it is very important to treat this effect properly. In order to determine the region where the $^1S_0$- or $^3P_2$-superfluid state exists in neutron-star matter, we must take into account that the realistic M^* is strongly density-dependent. In the calculation in II, we have simply adopted the effective mass approximation in $\tilde{\varepsilon}_k$ (the single-particle energy measured from the Fermi surface) and have not taken into account the density-dependence of M^*. In this paper, we take into account the effect of one-body potential $V_n(k)$ on $\tilde{\varepsilon}_k$ as $\tilde{\varepsilon}_k=\hbar^2(k^2-k_F^2)/2M+V_n(k)-V_n(k_F)$ and the density-dependence of $V_n(k)$ (or corresponding M^*). For $V_n(k)$ we use the potentials given in Table I,

Table I. One-body potential $V_n(k)$, which reproduces the potential values calculated for $k<k_F$ by Ikeuchi et al. and tends to zero as $k\to\infty$. The realistic effective mass parameters m^* are also shown.

E_F(MeV)	(10^{14}gcm^{-3})	$V_n(k)$ (MeV)	$m^*(=M^*/M)$
8	0.1	$-4.71\exp(-0.13k^2)$	0.98
16	0.4	$-9.95\exp(-0.15k^2)$	0.95
23	0.7	$-13.05\exp(-0.10k^2)-3.0\exp(-0.25k^2)$	0.93
30	1.0	$-18.11\exp(-0.10k^2)-4.06\exp(-0.28k^2)$	0.91
39	1.5	$-26.93\exp(-0.10k^2)-3.30\exp(-0.30k^2)$	0.89
45	1.8	$-32.34\exp(-0.13k^2)-5.19\exp(-0.10k^2)$	0.86
54	2.4	$-35.0\exp(-0.15k^2)-12.0\exp(-0.10k^2)$	0.82
76	4.0	$-41.0\exp(-0.15k^2)-29.0\exp(-0.10k^2)$	0.78
94	5.5	$-8.6\exp(-0.16k^2)$	0.75
120	7.9	$20.0\exp(-0.704k^2)-123.0\exp(-0.215k^2)$	0.70

which reproduce the potential values calculated for $k<k_F$ by Ikeuchi, Nagata, Mizutani and Nakazawa[6] and tend to zero as $k\to\infty$. Realistic values of the effective mass parameter $m^*(\equiv M^*/M)$ at $k=k_F$ are also shown there for several typical densities. For the low density such as $\rho\lesssim 7\times10^{12}$ gcm^{-3} we take $m^*=1$ in the calculation of the $^1S_0$-gap.

(2) The $^3P_2$-gap becomes negligibly small for the realistic nuclear force and the realistic density-dependence of M^*. In such a situation, the attractive effect of the $^3P_2$-$^3F_2$ coupling due to tensor force neglected in II is expected to play an important role to increase the $^3P_2$-gap.[3] In Fig. 1, the $^3P_2$-phase shifts for nucleon-nucleon scattering are shown as functions of the nucleon incident energy in Lab., $E_{N-N}^{(\mathrm{LAB})}$; those calculated from one of the existing semiphenomenological potentials, G3RS potential,[7] with and without the $^3P_2$-$^3F_2$ tensor coupling. From Fig. 1 we see that the effect of the $^3P_2$-$^3F_2$ tensor coupling brings only a small correction of several percent to the $^3P_2$-phase shifts. In the problem of pairing interaction

under consideration, however, for the realistic nuclear force and realistic M^* the ${}^3P_2$ interaction without this coupling is attractive just enough to bring such a critical situation that the ${}^3P_2$-gap begins to appear. In such a delicate situation, the effect of this coupling, although its effect to scattering is small, is considered to become very important because the energy gap is generally very sensitive to the strength of attractive force. We extend the pairing theory for the nonzero angular momentum states developed in I by taking into account this tensor coupling effect and solve the gap equation with the ${}^3P_2$-${}^3F_2$ tensor coupling.

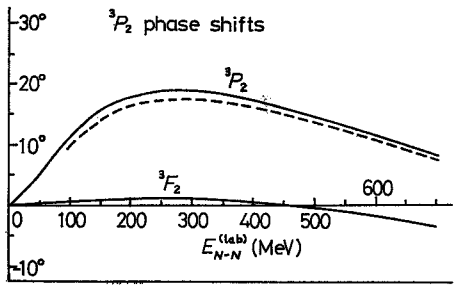

Fig. 1. ${}^3P_2$-phase shifts for nucleon-nucleon scattering as functions of the nucleon incident energy in Lab., $E_{N-N}^{(lab)}$ calculated from one of the existing semi-phenomenological potentials, G3RS potential,[7] with and without the tensor coupling:
——: with the ${}^3P_2-{}^3F_2$ tensor coupling,
- - - -: without the ${}^3P_2-{}^3F_2$ tensor coupling.

Calculations are done only with the two-nucleon OPEG ${}^3O-1$ potential[7] which has the OPEP-tail and 2 GeV Gaussian soft core, because this is one of the most realistic soft-core potentials currently used. We treat the simplest case with $m_j=0$ component only, i.e., Sol. 2-type among the five solutions discussed in II, since all of these have almost the same values of the ${}^3P_2$-gap and Sol. 2 belongs to the class with the lower ground state energy among five solutions.[8]

In § 2, we extend the pairing theory along the line developed in I, and derive the gap equation with the ${}^3P_2$-${}^3F_2$ tensor coupling. In § 3, the results of calculation are shown and the properties of the gap equation with the ${}^3P_2$-${}^3F_2$ tensor coupling are investigated. § 4 is devoted to discussions.

§ 2. Gap equation with the tensor coupling

The formulation given in this section is parallel with that in I, and the gap equation with the ${}^3P_2$-${}^3F_2$ tensor coupling is obtained. The notation follows those of I. As in I, we take the model Hamiltonian with a pair interaction as follows:

$$H_{\text{model}}=\sum_{k\sigma}\tilde{\varepsilon}_k C^*_{k\sigma}C_{k\sigma}+\tfrac{1}{2}\sum_{kk'}\sum_{\text{spin}}\langle \boldsymbol{k}'\sigma_1', -\boldsymbol{k}'\sigma_2'|V|\boldsymbol{k}\sigma_1, -\boldsymbol{k}\sigma_2\rangle \times C^*_{k'\sigma_1'}C^*_{-k'\sigma_2'}C_{k\sigma_2}C_{-k\sigma_1}. \tag{2·1}$$

On defining a boson operator, $b^{*\lambda}_{lm_j}(k)$, representing a pair with relative momentum k and angular-momentum quantum numbers $\lambda\equiv(s,j)$, l and m_j by

$$b^{*\lambda}_{lm_j}(k)\equiv\frac{1}{\sqrt{2}}\sum_{\sigma_1\sigma_2}\left(\frac{1}{2}\,\frac{1}{2}\,\sigma_1\sigma_2|sm_s\right)(slm_sm_l|jm_j)\int d\hat{k}Y_{lm_l}(\hat{k})C^*_{k\sigma_1}C^*_{-k\sigma_2} \tag{2·2}$$

and using

$$C^*_{k\sigma_1}C^*_{-k\sigma_2}=\sqrt{2}\sum_{\lambda l m_j}(\tfrac{1}{2}\tfrac{1}{2}\sigma_1\sigma_2|sm_s)\,(slm_sm_l|jm_j)\,b^{*\lambda}_{lm_j}(k)\,Y^*_{lm_l}(\hat{k}), \tag{2·3}$$

we have

$$H_{\text{model}}=\sum_{k\sigma}\tilde{\varepsilon}_kC^*_{k\sigma}C_{k\sigma}+\frac{(4\pi)^2}{\Omega}\sum_k\sum_{k'}\sum_{\lambda ll'}(i)^{l'-l}\langle k'|V_\lambda{}^{l'l}|k\rangle\sum_{m_j}b^{*\lambda}_{l'm_j}(k')\,b^{\lambda}_{lm_j}(k). \tag{2·4}$$

As discussed in I, if the attractive interaction is dominant in a particular pair state λ, superfluidity is mainly determined by this λ-state pair interaction and we can consider a more restricted model Hamiltonian with the λ-pair interaction only:

$$H_\lambda=\sum_{k\sigma}\tilde{\varepsilon}_kC^*_{k\sigma}C_{k\sigma}+\frac{(4\pi)^2}{\Omega}\sum_k\sum_{k'}\sum_{l'l}(i)^{l'-l}\langle k'|V_\lambda{}^{l'l}|k\rangle\sum_{m_j}b^{*\lambda}_{l'm_j}(k')\,b^{\lambda}_{lm_j}(k), \tag{2·4′}$$

where

$$\begin{cases}\langle k'|V_\lambda{}^{l'l}|k\rangle\equiv\int r^2dr\,j_{l'}(k'r)\,V_\lambda{}^{l'l}(r)\,j_l(kr),\\ V_\lambda{}^{l'l}(r)\equiv\int d\Omega_r\,\mathcal{Y}^{*\lambda}_{l'm_j}(1,2)\,V_{12}(r)\,\mathcal{Y}^{\lambda}_{lm_j}(1,2),\\ \mathcal{Y}^{\lambda}_{lm_j}(1,2)=\sum_{m_s+m_l=m_j}(slm_sm_l|jm_j)\,Y_{lm_l}(\hat{r})\,\chi_{sm_s}(1,2).\end{cases} \tag{2·5}$$

The coupled state results from the fact that the matrix element, $\langle k'|V_\lambda{}^{l'l}|k\rangle$ does not vanish for $l=j\pm1$, $l'=j\pm1$ through tensor force in $V_{12}(r)$ and the sum for l, l' in Eq. (2·4′) is taken for $j\pm1$. For $j=2$, $s=1$ and $l=1$ and 3 correspond to the ${}^3P_2$ and ${}^3F_2$ states, respectively. We define an operator S in the following way:

$$S=-i\sum_k\sum_{m_j,\,l=j\pm1}\{\phi^\lambda_{lm_j}(k)\,b^{*\lambda}_{lm_j}(k)-\phi^{*\lambda}_{lm_j}(k)\,b^{\lambda}_{lm_j}(k)\}. \tag{2·6}$$

This operator is different from S in Eq. (3·3) in I in the point that it should include the l-sum in order to take into account the tensor coupling. The unitary transformation (a generalized Bogoliubov transformation) is given in the form

$$|\Psi_0\rangle=e^{iS}|\Phi_0\rangle, \tag{2·7}$$

where $|\Phi_0\rangle$ is the Fermi-gas ground state and $|\Psi_0\rangle$ the ground state for quasiparticles. Then,

$$iS=\tfrac{1}{2}\sum_{k\sigma_1\sigma_2}\{\theta_\lambda(k\sigma_1\sigma_2)C^*_{k\sigma_1}C^*_{-k\sigma_2}-\theta_\lambda{}^*(k\sigma_1\sigma_2)C_{-k\sigma_2}C_{k\sigma_1}\}, \tag{2·8}$$

$$\theta_\lambda(k\sigma_1\sigma_2)=\sqrt{2}\sum_{m_j}\sum_{l=j\pm1}(\tfrac{1}{2}\tfrac{1}{2}\sigma_1\sigma_2|sm_s)\,(slm_sm_l|jm_j)\,Y_{lm_l}(\hat{k})\,\phi^\lambda_{lm_j}(k). \tag{2·9}$$

We write $C_{k\sigma}$, $C^*_{k\sigma}$ and θ_λ in the following matrix forms:

$$\boldsymbol{C}_{\boldsymbol{k}}\equiv\begin{pmatrix}C_{\boldsymbol{k}\uparrow}\\ C_{\boldsymbol{k}\downarrow}\end{pmatrix},\qquad \boldsymbol{C}_{\boldsymbol{k}}{}^{*}\equiv\begin{pmatrix}C^{*}_{\boldsymbol{k}\uparrow}\\ C^{*}_{\boldsymbol{k}\downarrow}\end{pmatrix},$$

$$\boldsymbol{\theta}_{\lambda}(\boldsymbol{k})\equiv\{\theta_{\lambda}(\boldsymbol{k}\sigma_1\sigma_2)\}=\begin{pmatrix}\theta_{\lambda}(\boldsymbol{k}\uparrow\uparrow) & \theta_{\lambda}(\boldsymbol{k}\uparrow\downarrow)\\ \theta_{\lambda}(\boldsymbol{k}\downarrow\uparrow) & \theta_{\lambda}(\boldsymbol{k}\downarrow\downarrow)\end{pmatrix}. \tag{2·10}$$

When $\boldsymbol{\theta}_{\lambda}(\boldsymbol{k})$ is given, we can obtain the quasiparticle operators $\boldsymbol{\alpha}_{\boldsymbol{k}}$ in the matrix representation in the formally identical way discussed in I:

$$\begin{aligned}\boldsymbol{\alpha}_{\boldsymbol{k}}&=e^{iS}\boldsymbol{C}_{\boldsymbol{k}}e^{-iS}\\ &=U_{\lambda}(\boldsymbol{k})\boldsymbol{C}_{\boldsymbol{k}}-V_{\lambda}(\boldsymbol{k})\boldsymbol{C}^{*}_{-\boldsymbol{k}}\,,\\ \boldsymbol{\alpha}_{\boldsymbol{k}}{}^{*}&=e^{iS}\boldsymbol{C}_{\boldsymbol{k}}{}^{*}e^{-iS}\\ &=U_{\lambda}{}^{*}(\boldsymbol{k})\boldsymbol{C}_{\boldsymbol{k}}{}^{*}-V_{\lambda}{}^{*}(\boldsymbol{k})\boldsymbol{C}_{-\boldsymbol{k}}\end{aligned} \tag{2·11}$$

with

$$\begin{aligned}U_{\lambda}(\boldsymbol{k})&=\cos\boldsymbol{\theta}_{\lambda}{}'(\boldsymbol{k}),\\ V_{\lambda}(\boldsymbol{k})&=\boldsymbol{\theta}_{\lambda}{}'^{-1}(\boldsymbol{k})\sin\boldsymbol{\theta}_{\lambda}{}'(\boldsymbol{k})\boldsymbol{\theta}_{\lambda}(\boldsymbol{k}),\end{aligned} \tag{2·12}$$

where $\boldsymbol{\theta}_{\lambda}{}'(\boldsymbol{k})$ is the Hermite matrix defined by

$$\boldsymbol{\theta}_{\lambda}{}'^{2}(\boldsymbol{k})=\boldsymbol{\theta}_{\lambda}(\boldsymbol{k})\boldsymbol{\theta}_{\lambda}{}^{\dagger}(\boldsymbol{k}). \tag{2·13}$$

Here, $\boldsymbol{\theta}_{\lambda}{}'(\boldsymbol{k})$ in this paper is different from $\boldsymbol{\theta}_{\lambda}{}'(\boldsymbol{k})$ defined in I in the point that it contains the summation of $l(=j\pm1)$ through $\theta_{\lambda}(\boldsymbol{k}\sigma_1\sigma_2)$ in Eq. (2·9) due to the tensor coupling. But, as is generally shown in Appendix A, $\boldsymbol{\theta}_{\lambda}{}'(\boldsymbol{k})$ with the tensor coupling is written in the form proportional to unit matrix:

$$\boldsymbol{\theta}_{\lambda}{}'(\boldsymbol{k})=\pm\theta_{D}(\boldsymbol{k})\times\boldsymbol{1}\,, \tag{2·14}$$

where $\theta_{D}(\boldsymbol{k})$ is given in Appendix A. The Fermion commutation relations for C's are transformed into those for α's:

$$\{\alpha_{\boldsymbol{k}\rho},\,\alpha^{*}_{\boldsymbol{k}'\rho'}\}=\delta_{\boldsymbol{k}\rho,\boldsymbol{k}'\rho'},\quad \{\alpha_{\boldsymbol{k}\rho},\,\alpha_{\boldsymbol{k}'\rho'}\}=\{\alpha^{*}_{\boldsymbol{k}\rho},\,\alpha^{*}_{\boldsymbol{k}'\rho'}\}=0\,. \tag{2·15}$$

Using Eq. (2·14) and the properties of $\boldsymbol{\theta}_{\lambda}(\boldsymbol{k})$, we can show that the conditions (3·13a$\sim$d) in I are also satisfied by the U_{λ} and V_{λ} defined by Eq. (2·12). This is shown in Appendix B. The inverse transformation can be written in the same form as Eq. (3·14) in I as follows:

$$\begin{aligned}\boldsymbol{C}_{\boldsymbol{k}}&=U_{\lambda}{}^{\dagger}(\boldsymbol{k})\boldsymbol{\alpha}_{\boldsymbol{k}}-\tilde{V}_{\lambda}(-\boldsymbol{k})\boldsymbol{\alpha}^{*}_{-\boldsymbol{k}}=U_{\lambda}(\boldsymbol{k})\boldsymbol{\alpha}_{\boldsymbol{k}}+V_{\lambda}(\boldsymbol{k})\boldsymbol{\alpha}^{*}_{-\boldsymbol{k}}\,,\\ \boldsymbol{C}^{*}_{-\boldsymbol{k}}&=\tilde{U}_{\lambda}(-\boldsymbol{k})\boldsymbol{\alpha}^{*}_{-\boldsymbol{k}}-V_{\lambda}{}^{\dagger}(\boldsymbol{k})\boldsymbol{\alpha}_{\boldsymbol{k}}=\tilde{U}_{\lambda}(\boldsymbol{k})\boldsymbol{\alpha}^{*}_{-\boldsymbol{k}}-V_{\lambda}{}^{\dagger}(\boldsymbol{k})\boldsymbol{\alpha}_{\boldsymbol{k}}\,.\end{aligned} \tag{2·16}$$

Using Eq. (2·16), boson operator $b^{*\lambda}_{lm_j}(k')$ becomes

$$\begin{aligned}b^{*\lambda}_{lm_j}(k')=\frac{1}{\sqrt{2}}\int d\hat{k}'\sum_{\rho\rho'}\{&(U_{\lambda}(\boldsymbol{k}')G^{\lambda}_{lm_j}(\hat{k}')\tilde{U}_{\lambda}(\boldsymbol{k}'))_{\rho\rho'}\alpha^{*}_{\boldsymbol{k}'\rho}\alpha^{*}_{-\boldsymbol{k}'\rho'}\\ &-(U_{\lambda}(\boldsymbol{k}')G^{\lambda}_{lm_j}(\hat{k}')V_{\lambda}{}^{\dagger}(\boldsymbol{k}'))_{\rho\rho'}\alpha^{*}_{\boldsymbol{k}'\rho}\alpha_{\boldsymbol{k}'\rho'}\end{aligned}$$

$$+(V_\lambda^\dagger(\boldsymbol{k}')G^\lambda_{lm_j}(\hat{k}')\tilde{U}_\lambda(\boldsymbol{k}'))_{\rho\rho'}\alpha_{-\boldsymbol{k}'\rho}\alpha^*_{-\boldsymbol{k}'\rho'}$$
$$-(V_\lambda^\dagger(\boldsymbol{k}')G^\lambda_{lm_j}(\hat{k}')V_\lambda^\dagger(\boldsymbol{k}'))_{\rho\rho'}\alpha_{-\boldsymbol{k}'\rho}\alpha_{\boldsymbol{k}'\rho'}\}, \quad (2\cdot17)$$

where

$$G^\lambda_{lm_j}(\hat{k}')\equiv(\tfrac{1}{2}\tfrac{1}{2}\sigma_1\sigma_2|sm_s)\,(slm_sm_j-m_s|jm_j)\,Y_{l,m_j-m_s}(\hat{k}') \quad (2\cdot18)$$

is the 2×2 matrix in spin space.

In terms of Eq. (2·17) and the corresponding equation for $b^\lambda_{lm_j}(k)$, H_λ is rewritten by quasiparticle operators α, α^* and is separated into H_{00} (constant terms), $H_{11}(\alpha^*\alpha$ term), $H_{20}(\alpha^*\alpha^*, \alpha\alpha$ terms) and the higher-order terms with respect to quasiparticle operators. On neglecting the terms $\sim O(1/\Omega)$ and the higher-order terms, H_{20} becomes as follows:

$$H_{20}=\sum_{\boldsymbol{k}}\sum_{\rho\rho'}\alpha^*_{\boldsymbol{k}\rho}\alpha^*_{-\boldsymbol{k}\rho'}\Big\{\tilde{\varepsilon}_k(U_\lambda(\boldsymbol{k})V_\lambda(\boldsymbol{k}))_{\rho\rho'}+\frac{(4\pi)^2}{\Omega}\frac{(-)^{1-s}}{2}\sum_{\boldsymbol{k}'}\sum_{ll'}(i)^{l'-l}$$
$$\times\langle k|V_\lambda{}^{l'l}|k'\rangle\sum_{m_j}\mathrm{Tr}[\tilde{U}_\lambda(\boldsymbol{k}')G^{*\lambda}_{lm_j}(\hat{k}')V_\lambda(\boldsymbol{k}')](U_\lambda(\boldsymbol{k})G^\lambda_{l'm_j}(\hat{k})$$
$$\times\tilde{U}_\lambda(\boldsymbol{k}))_{\rho\rho'}-\frac{(4\pi)^2}{\Omega}\frac{(-)^{1-s}}{2}\sum_{\boldsymbol{k}'}\sum_{l'l}(i)^{l'-l}\langle k'|V_\lambda{}^{l'l}|k\rangle$$
$$\times\sum_{m_j}\mathrm{Tr}[V_\lambda^\dagger(\boldsymbol{k}')G^\lambda_{l'm_j}(\hat{k}')\tilde{U}_\lambda(\boldsymbol{k}')](V_\lambda(\boldsymbol{k})\tilde{G}^{*\lambda}_{lm_j}(\hat{k})V_\lambda(\boldsymbol{k}))_{\rho\rho'}\}$$
$$+\text{Hermitian conjugate.} \quad (2\cdot19)$$

Then, by the use of the relation

$$\langle k|V_\lambda{}^{l'l}|k'\rangle\equiv\langle k'|V_\lambda{}^{ll'}|k\rangle$$

and rewriting l by l' and l' by l in the second term in the curly bracket on the right-hand side of Eq. (2·19), we obtain

$$H_{20}=\sum_{\boldsymbol{k}}\sum_{\rho\rho'}\alpha^*_{\boldsymbol{k}\rho}\alpha^*_{-\boldsymbol{k}\rho}\Big\{\tilde{\varepsilon}_k(U_\lambda(\boldsymbol{k})V_\lambda(\boldsymbol{k}))_{\rho\rho'}+\frac{(4\pi)^2}{\Omega}\frac{(-)^{1-s}}{2}$$
$$\times\sum_{\boldsymbol{k}'}\sum_{ll'}(i)^{l'-l}\langle k'|V_\lambda{}^{l'l}|k\rangle\sum_{m_j}\{\mathrm{Tr}[\tilde{U}_\lambda(\boldsymbol{k}')G^{*\lambda}_{l'm_j}(\hat{k}')V_\lambda(\boldsymbol{k}')]$$
$$\times(U_\lambda(\boldsymbol{k})G^\lambda_{lm_j}(\hat{k})\tilde{U}_\lambda(\boldsymbol{k}))_{\rho\rho'}-\mathrm{Tr}[V_\lambda^\dagger(\boldsymbol{k}')G^\lambda_{l'm_j}(\hat{k}')\tilde{U}_\lambda(\boldsymbol{k}')]$$
$$\times(V_\lambda(\boldsymbol{k})\tilde{G}^{*\lambda}_{lm_j}(\hat{k})V_\lambda(\boldsymbol{k}))_{\rho\rho'}\}\Big\}+\text{Hermitian conjugate}, \quad (2\cdot19')$$

where we have used the relation that $|l'-l|$ is even. The elimination of the dangerous term H_{20} leads to the equation

$$2\tilde{\varepsilon}_kU_\lambda(\boldsymbol{k})V_\lambda(\boldsymbol{k})=\sum_{l,m_j}\{\Delta^\lambda_{lm_j}(k)U_\lambda(\boldsymbol{k})G^\lambda_{lm_j}(\hat{k})\tilde{U}_\lambda(\boldsymbol{k})$$
$$-\Delta^{*\lambda}_{lm_j}(k)V_\lambda(\boldsymbol{k})\tilde{G}^{*\lambda}_{lm_j}(\hat{k})V_\lambda(\boldsymbol{k})\}$$
$$=U_\lambda(\boldsymbol{k})\Delta^\lambda(\boldsymbol{k})\tilde{U}_\lambda(\boldsymbol{k})-V_\lambda(\boldsymbol{k})\Delta^{\lambda\dagger}(\boldsymbol{k})V_\lambda(\boldsymbol{k}), \quad (2\cdot20)$$

where

$$\Delta_{lm_j}^{\lambda}(k) = -\frac{(4\pi)^2}{\Omega}(-)^{1-s}\sum_{k'}\sum_{l'}(i)^{l'-l}\langle k'|V_{\lambda}^{l'l}|k\rangle \times \mathrm{Tr}[\tilde{U}_{\lambda}(\boldsymbol{k}')G_{l'm_j}^{*\lambda}(\hat{k}')V(\boldsymbol{k}')] \qquad (2\cdot21)$$

and

$$\boldsymbol{\Delta}^{\lambda}(\boldsymbol{k}) = \sum_{lm_j}\Delta_{lm_j}^{\lambda}(k)G_{lm_j}^{\lambda}(\hat{k}) \qquad (2\cdot22)$$

is the 2×2 matrix in spin space. By the use of the relation (2·14) that $\boldsymbol{\theta}_{\lambda}'(\boldsymbol{k})$ is proportional to unit matrix, we can solve Eq. (2·20) in the same way as shown for Eqs. (4·19)$\sim$(4·24) in I and obtain the following gap equation with the tensor coupling:

$$\Delta_{lm_j}^{\lambda}(k) = -\frac{1}{\pi}(-)^{1-s}\int k'^2dk'\int d\hat{k}'\sum_{l'}(i)^{l'-l}\langle k'|V_{\lambda}^{l'l}|k\rangle \times \sum_{l''\mu}\Delta_{l''\mu}^{\lambda}(k')\mathrm{Tr}[G_{l'm_j}^{*\lambda}(\hat{k}')G_{l''\mu}^{\lambda}(\hat{k}')]/\sqrt{\tilde{\varepsilon}_{k'}^2+D_{\lambda}^2(\boldsymbol{k}')}, \qquad (2\cdot23)$$

where

$$D_{\lambda}^2(\boldsymbol{k}') = \tfrac{1}{2}\mathrm{Tr}(\boldsymbol{\Delta}^{\lambda\dagger}(\boldsymbol{k}')\boldsymbol{\Delta}^{\lambda}(\boldsymbol{k}')) = \tfrac{1}{2}\sum_{ll'}\sum_{m_jm_{j'}}\Delta_{lm_j}^{\lambda}(k')\Delta_{l'm_{j'}}^{\dagger\lambda}(k')\mathrm{Tr}[G_{lm_j}^{\lambda}(\hat{k}')G_{l'm_{j'}}^{\dagger\lambda}(\hat{k}')]. \qquad (2\cdot24)$$

Here we write down explicitly the energy-gap equation for the $({}^3P_2+{}^3F_2)$-state ($\lambda(j=2, s=1)$ and $l=1, 3$). For the simplest case ($m_j=0$ component only), the ${}^3P_2$ energy-gap function $\Delta_{10}^{\lambda}(k)$ and ${}^3F_2$-one $\Delta_{30}^{\lambda}(k)$ satisfy the following gap equation with the ${}^3P_2$-${}^3F_2$ tensor coupling (V_{λ}^{31} and V_{λ}^{13}):

$$\Delta_{10}^{\lambda}(k) = -\frac{1}{\pi}\int k'^2dk'\langle k'|V_{\lambda}^{11}|k\rangle\int d\hat{k}'\{\Delta_{10}^{\lambda}(k')f(\theta)+\Delta_{30}^{\lambda}(k')g(\theta)\}/E_{\boldsymbol{k}'} + \frac{1}{\pi}\int k'^2dk'\langle k'|V_{\lambda}^{31}|k\rangle\int d\hat{k}'\{\Delta_{10}^{\lambda}(k')g(\theta)+\Delta_{30}^{\lambda}(k')h(\theta)\}/E_{\boldsymbol{k}'}, \qquad (2\cdot25a)$$

$$\Delta_{30}^{\lambda}(k) = \frac{1}{\pi}\int k'^2dk'\langle k'|V_{\lambda}^{13}|k\rangle\int d\hat{k}'\{\Delta_{10}^{\lambda}(k')f(\theta)+\Delta_{30}^{\lambda}(k')g(\theta)\}/E_{\boldsymbol{k}'} - \frac{1}{\pi}\int k'^2dk'\langle k'|V_{\lambda}^{33}|k\rangle\int d\hat{k}'\{\Delta_{10}^{\lambda}(k')g(\theta)+\Delta_{30}^{\lambda}(k')h(\theta)\}/E_{\boldsymbol{k}'}, \qquad (2\cdot25b)$$

where

$$\begin{cases} f(\theta) = \dfrac{1}{8\pi}(1+3\cos^2\theta), \\ g(\theta) = \dfrac{\sqrt{6}}{64\pi}(1-7\cos^2\theta+5\sin\theta\sin3\theta-10\cos\theta\cos3\theta), \end{cases}$$

$$\begin{cases} h(\theta)=\dfrac{3}{128\pi}(13+4\cos^2\theta+5\sin\theta\sin 3\theta+15\cos\theta\cos 3\theta), \\ E_{k'}=\sqrt{\tilde{\varepsilon}_{k'}^2+D_\lambda^2(k')} \end{cases} \tag{2·26}$$

and

$$D_\lambda^2(k')=\tfrac{1}{2}f(\theta)\,(\Delta_{10}^\lambda(k'))^2+\tfrac{1}{2}h(\theta)\,(\Delta_{30}^\lambda(k'))^2+g(\theta)\,\Delta_{10}^\lambda(k')\,\Delta_{30}^\lambda(k'). \tag{2·27}$$

Here θ is the polar angle of the vector k'. Equations (2·25a)$\sim$(2·27) are solved by an iterative method.

For $^1S_0$-pairing ($j=0, s=0, l=0$) we solve the following well-known energy-gap equation:

$$\delta(k)=-\frac{1}{\pi}\int k'^2dk'\langle k'|V_{^1S_0}|k\rangle\delta(k')/\sqrt{\tilde{\varepsilon}_{k'}^2+\delta^2(k')} \tag{2·28}$$

by the same method, where $\delta(k)$ is the $^1S_0$ energy-gap function and $V_{^1S_0}$ is a nucleon-nucleon potential in the $^1S_0$ state.

§ 3. Calculated results and the properties of the gap equation with the $^3P_2$-$^3F_2$ tensor coupling

§ 3-1 *Calculated results*

In Fig. 2 the values of the $^3P_2$-gap at $k=k_F$, $\Delta_{10}^\lambda(k_F)$ (with the tensor coupling), and that of $^1S_0$, $\delta(k_F)$, obtained using the realistic density dependence of the effective mass parameter, $m^*(M^*/M)$ are plotted as functions of the density of the neutron-star matter ρ or Fermi energy E_F. The density dependence of m^* is indicated by arrows in Fig. 2. The critical temperature, T_c, calculated from the relation[3]

$$\begin{aligned} K_BT_c &\simeq 0.57\times\Delta_{10}^\lambda(k_F)/\sqrt{2}\Gamma_0\,, \quad \ln\Gamma_0=1.22 \quad \text{for } ^3P_2, \\ &\simeq 0.57\times\delta(k_F) \quad \text{for } ^1S_0 \end{aligned} \tag{3·1}$$

is shown in Fig. 3. The $^1S_0$- and $^3P_2$-superfluid states exist in the region $\rho\simeq(1.0\times10^{11}\sim1.5\times10^{14})\,\mathrm{gcm}^{-3}$ and $\rho\simeq(2\sim8)\times10^{14}\,\mathrm{gcm}^{-3}$, respectively. The maximum $^3P_2$-gap takes place near the region $\rho\simeq4\times10^{14}\,\mathrm{gcm}^{-3}$ and its value is about 0.6 MeV. To compare the $^3P_2$-gap with $^1S_0$-one quantitatively, T_c in Fig. 3 should be used because of the angular dependence of the $^3P_2$-gap.

In our previous calculations neglecting the $^3P_2$-$^3F_2$ tensor coupling, we have found that the $^3P_2$-gap was very small ($\sim$0.02 MeV) for $m^*=0.8$, $E_F=75$ MeV although it was sufficiently large ($\sim$2.2 MeV) for $m^*=1$, $E_F=75$ MeV.[3] From these it is known that the $^3P_2$-gap is very sensitive to m^*. Realistic m^* (m^* in actual neutron-star) is strongly density-dependent and becomes small as ρ increases ($m^*=0.82\to0.70$ for $\rho=(2\to8)\times10^{14}\,\mathrm{gcm}^{-3}$). Therefore, whether the $^3P_2$-gap exists in neutron-star or not is considered to be in a critical situation for realistic m^* and without the $^3P_2-{}^3F_2$ tensor-coupling effect, which is attractive

and increases the ${}^3P_2$-gap. In fact, without this coupling, we have negligibly small ${}^3P_2$-gap in neutron-star matter for any realistic value of m^* or $V_n(k)$:

$$\Delta_{10}'^{\lambda}(k_F) \simeq 0 \text{ MeV} \quad \text{for } \rho \simeq 2\times10^{14}\text{gcm}^{-3} \ (E_F \simeq 54 \text{ MeV}),\ m^* \simeq 0.82,$$
$$< 0.008 \text{ MeV} \quad \text{for } \rho \simeq 4\times10^{14}\text{gcm}^{-3} \ (E_F \simeq 76 \text{ MeV}),\ m^* \simeq 0.78,$$
$$< 0.003 \text{ MeV} \quad \text{for } \rho \simeq 6\times10^{14}\text{gcm}^{-3} \ (E_F \simeq 94 \text{ MeV}),\ m^* \simeq 0.75,$$

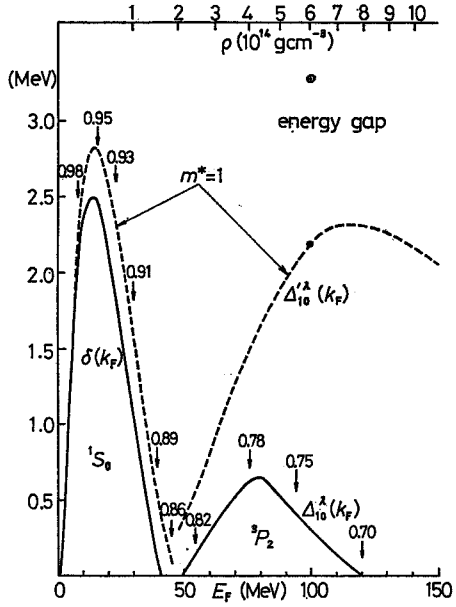

Fig. 2. The ${}^1S_0$- and ${}^3P_2$-gaps as functions of the density of neutron-star matter ρ or Fermi energy E_F.
——: The ${}^3P_2$-gap at $k=k_F$, $\Delta_{10}{}^{\lambda}(k_F)$ (with the tensor coupling), and that of ${}^1S_0$, $\delta(k_F)$, for the realistic density dependence of the effective mass parameter, $m^*(\equiv M^*/M)$,
- - - -: The ${}^3P_2$-gap at $k=k_F$, $\Delta_{10}{}'^{\lambda}(k_F)$ (without the tensor coupling), and $\delta(k_F)$ for $m^*=1$,
●: $\Delta_{10}{}'^{\lambda}(k_F)$ for $m^*=1$ and $E_F=100$MeV,
⊙: $\Delta_{10}{}^{\lambda}(k_F)$ for $m^*=1$ and $E_F=100$MeV,
↓: the values of m^*.

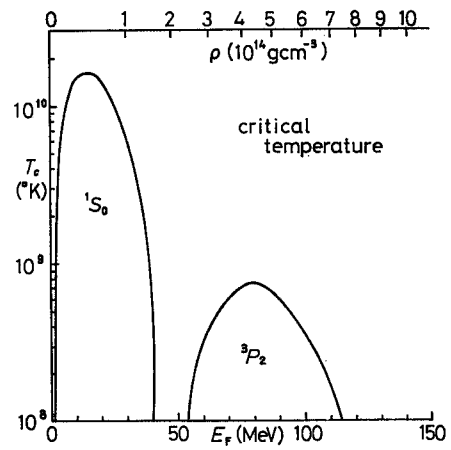

Fig. 3. Density dependence of the critical temperature T_c.

where $\Delta_{10}'^{\lambda}(k_F)$ denotes the ${}^3P_2$-gap at $k=k_F$ without tensor coupling. But with tensor coupling, we have the ${}^3P_2$-gap ($\sim$0.5 MeV) shown in Fig. 2. From those we can say that for the case with realistic m^* and ρ, the tensor-coupling effect is especially important. For larger values of m^*, for example, if we put $m^*=1$ at $E_F=100$ MeV, $\Delta_{10}'^{\lambda}(k_F)$ is 2.22 MeV, while $\Delta_{10}^{\lambda}(k_F)$ is 3.28 MeV as is shown in Fig. 2. In such a case that the gap is large, the tensor-coupling effect has a role to increase the ${}^3P_2$-gap by a factor $\sim$1.5. In § 3-2, we investigate the mechanism that the ${}^3P_2$-${}^3F_2$ tensor coupling increases the ${}^3P_2$-gap.

§ 3-2 *The properties of the gap equation with the ${}^3P_2-{}^3F_2$ tensor coupling*

In Fig. 4, the nucleon-nucleon interaction potential $V_\lambda{}^{11}(r)=V_{{}^3P_2}$, $V_\lambda{}^{33}(r)$

$=V_{^3F_2}$ and $V_\lambda^{31}(r)=V_\lambda^{13}(r)=V_{\text{couple}}$ are shown in the case of OPEG $^3O-1$ potential.[7] $V_{^3P_2}$ is strongly attractive for $r\gtrsim 0.6\,\text{fm}^{-1}$ due to the medium-range spin-orbit force and turns repulsive for $r\lesssim 0.6\,\text{fm}^{-1}$ due to the repulsive core. $V_{^3F_2}$ is repulsive for $r\lesssim 1.6\,\text{fm}^{-1}$ and has a weak attractive tail for $r\gtrsim 1.6\,\text{fm}^{-1}$ due to the long-range nature of the tensor force. V_{couple} is positive for all r mainly due to the OPE (one-pion-exchange) tensor potential. The matrix elements of these potentials $\langle k'|V_\lambda^{l'l}|k_F\rangle$ at $k=k_F$ are shown in Fig. 5. These matrix

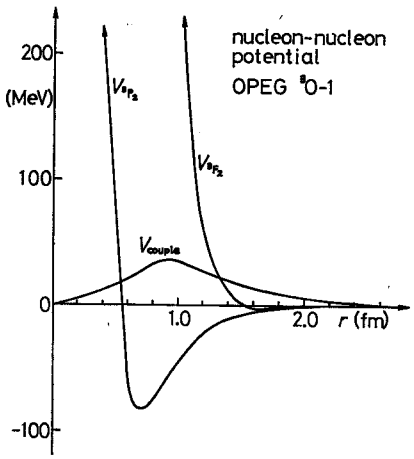

Fig. 4. Nucleon-nucleon interaction potential $V_\lambda^{l'l}(r)$ in the case of OPEG $^3O-1$ potential:[7]
$V_\lambda^{11}(r)=V_{^3P_2}$, (without the $^3P_2$-$^3F_2$ tensor coupling)
$V_\lambda^{33}(r)=V_{^3F_2}$, (without the $^3P_2$-$^3F_2$ tensor coupling)
$V_\lambda^{31}(r)=V_\lambda^{13}(r)=V_{\text{couple}}$. (the $^3P_2$-$^3F_2$ tensor coupling term)

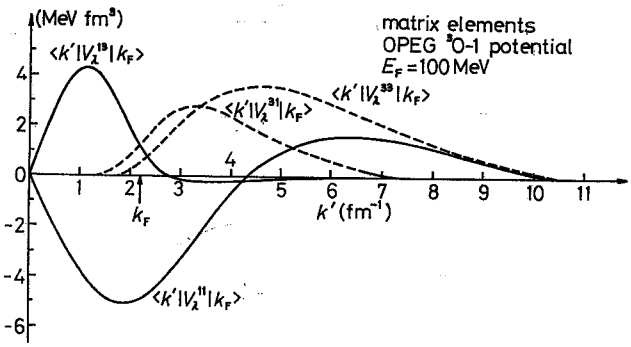

Fig. 5. Matrix elements of $V_\lambda^{l'l}(r)$, $\langle k'|V_\lambda^{l'l}|k_F\rangle$, at $k=k_F$ as functions of k' for $m^*=1$ and $E_F=100$MeV.

elements for $k'\simeq k_F$ play an important role to the existence of the energy gap because the integration over k' in the gap equation acts mainly for $k'\simeq k_F$. From Fig. 5, we know that only $\langle k'|V_\lambda^{11}|k_F\rangle$ is negative for $k'\simeq k_F$ and others, i.e., $\langle k'|V_\lambda^{13}|k_F\rangle$, $\langle k'|V_\lambda^{31}|k_F\rangle$ and $\langle k'|V_\lambda^{33}|k_F\rangle$ are positive for $k'\simeq k_F$.

Here we turn to investigation of the structure of the gap equation with the $^3P_2$-$^3F_2$ tensor coupling, i.e., Eqs. (2·25)$\sim$(2·27). In Eqs. (2·25 a, b), the contributions of $\Delta_{10}^\lambda(k')g(\theta)$ and $\Delta_{30}^\lambda(k')g(\theta)$ are small compared with that of $\Delta_{10}^\lambda(k')f(\theta)$ and $\Delta_{30}^\lambda(k')h(\theta)$ after the angular integration over $\hat{k}'$. So we can approximately rewrite Eqs. (2·25a, b) at $k=k_F$ in the following forms:

$$\Delta_{10}^\lambda(k_F)\simeq -\frac{1}{\pi}\int k'^2dk'\langle k'|V_\lambda^{11}|k_F\rangle\int d\hat{k}'\Delta_{10}^\lambda(k')f(\theta)/E_{k'}$$
$$+\frac{1}{\pi}\int k'^2dk'\langle k'|V_\lambda^{31}|k_F\rangle\int d\hat{k}'\Delta_{30}^\lambda(k')h(\theta)/E_{k'}, \qquad (3\cdot 2a)$$

$$\Delta_{30}^\lambda(k_F)\simeq\frac{1}{\pi}\int k'^2dk'\langle k'|V_\lambda^{13}|k_F\rangle\int d\hat{k}'\Delta_{10}^\lambda(k')f(\theta)/E_{k'}$$

$$-\frac{1}{\pi}\int k'^2dk'\langle k'|V_\lambda^{33}|k_F\rangle\int d\hat{k}'\Delta_{30}^\lambda(k')h(\theta)/E_{k'}. \qquad (3\cdot 2b)$$

If the tensor coupling is absent, i.e., $V_\lambda^{31}=0$, the second term on the right-hand side of Eq. (3·2a) does not appear, which is the case of $m_J=0$ component only, i.e., Sol. 2 in II. With the tensor coupling, however, the second term appears and plays a role to increase the ${}^3P_2$-gap, $\Delta_{10}^\lambda(k_F)$. Roughly speaking, this is caused by the following mechanism of this gap equation. If $\Delta_{30}^\lambda(k')$ is positive for $k'\simeq k_F$ the second term integrated over k' contributes to increase $\Delta_{10}^\lambda(k_F)$ because the quantity $\langle k'|V_\lambda^{31}|k_F\rangle$ is positive for $k'\simeq k_F$ and the integration over k' acts mainly for $k'\simeq k_F$. Whether $\Delta_{30}^\lambda(k')$ has a role mentioned above is determined by the properties of Eq. (3·2b). As is shown in Fig. 4, both $\langle k'|V_\lambda^{13}|k_F\rangle$ and $\langle k'|V_\lambda^{33}|k_F\rangle$ are positive and of the same order. Therefore $\Delta_{10}^\lambda(k')\gg|\Delta_{30}^\lambda(k')|$ leads to the positive $\Delta_{30}^\lambda(k_F)$ in Eq. (3·2b). $\Delta_{30}^\lambda(k)$ also becomes positive for $k\simeq k_F$ for the same reason mentioned above and plays a role to increase $\Delta_{10}^\lambda(k_F)$ in Eq. (3·2a).

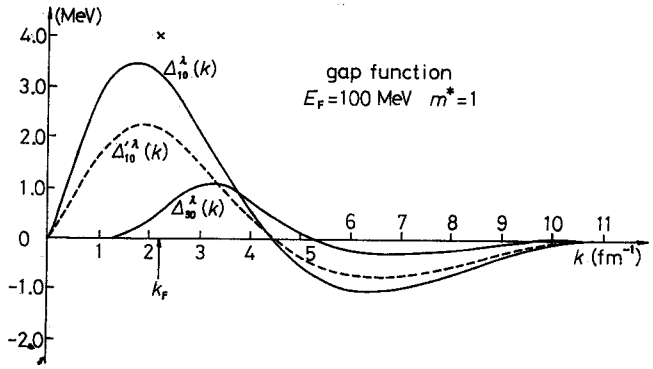

Fig. 6. The gap function with the ${}^3P_2$-${}^3F_2$ tensor coupling, $\Delta_{10}{}^\lambda(k)$, (${}^3P_2$) and $\Delta_{30}{}^\lambda(k)$, (${}^3F_2$) for $m^*=1$ and $E_F=100$MeV. The ${}^3P_2$-gap function without this coupling $\Delta_{10}{}^\lambda(k)$ for $m^*=1$ and $E_F=100$ MeV is also shown by the dotted lines for comparison. $\Delta_{10}{}^\lambda(k_F)$ obtained by using Mongan's potential is indicated by the cross.

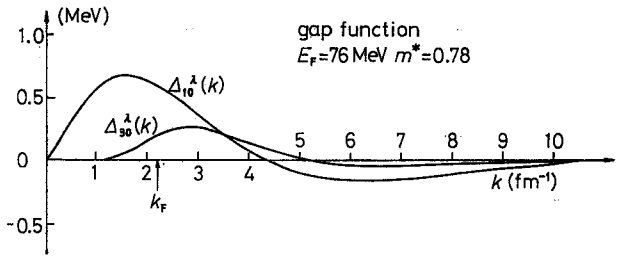

Fig. 7. The gap function with the ${}^3P_2-{}^3F_2$ tensor coupling, $\Delta_{10}{}^\lambda(k)$ and $\Delta_{30}{}^\lambda(k)$ for the realistic case with $m^*=0.78$ and $E_F=76$MeV. In this case, the gap function without this coupling $\Delta_{10}{}'^\lambda(k)$ becomes zero for all k and the ${}^3P_2$-gap cannot exist.

In fact, the coupled integral equations (2·25)$\sim$(2·27) are solved by an iterative method. The resulting gap function with the tensor coupling, $\Delta_{10}^{\lambda}(k)$ and $\Delta_{30}^{\lambda}(k)$, are shown in Fig. 6 in comparison with the gap function without the tensor coupling $\Delta_{10}'^{\lambda}(k)$ for $m^*=1$ and $E_F=100$ MeV. From these, $\Delta_{30}^{\lambda}(k)$ at $k \simeq k_F$ is seen to be surely positive, being consistent with the arguments mentioned above. $\Delta_{10}^{\lambda}(k)$ is increased by a factor $\sim$1.5 due to the effect of this tensor coupling. For the realistic case with $m^*=0.78$ and $E_F=76$ MeV, the $\Delta_{10}^{\lambda}(k)$ and $\Delta_{30}^{\lambda}(k)$ are shown in Fig. 7. In this case, the value of $\Delta_{10}'^{\lambda}(k)$ becomes zero for all k, and the $^3P_2$-gap cannot exist. These are the reason why the $^3P_2$-energy gap is increased by the $^3P_2$-$^3F_2$ tensor coupling. The qualitative feature of these results can be simulated by taking into account the reasonable density dependence of m^* on the $^3P_2$-gap calculated from a simple phenomenological, nonlocal separable potential. The calculated results of the $\Delta_{10}^{\lambda}(k_F)$ for $m^*=1$ and $E_F=100$ MeV in the case of Mongan's potential[8] is 4.01 MeV as is shown by the cross in Fig. 6. This value is a little larger than $\Delta_{10}^{\lambda}(k_F)=3.28$ MeV obtained by solving the gap equation with the $^3P_2$-$^3F_2$ tensor coupling. From these, we can say that a conventional way used to get the $^3P_2$-gap by the use of some effective potentials such as Mongan's[8] or Tabakin's[9] one is allowed as a rough estimate, if we suitably choose the correct density dependence of m^* shown in Fig. 2. $\Delta_{10}^{\lambda}(k_F)$ calculated from Mongan's potential for realistic density dependence of m^* is shown in Fig. 8 by dashed lines. In order to get more accurate results, it is necessary to solve the gap equation with the tensor coupling.

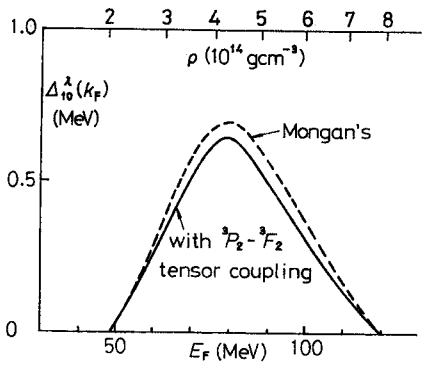

Fig. 8. The density dependence of $\Delta_{10}^{\lambda}(k_F)$ calculated by solving the gap equation with the $^3P_2$-$^3F_2$ tensor coupling for OPEG ^{3}O$-$1 in comparison with that obtained by the use of Mongan's effective $^3P_2$ potential and the density dependence of m^*.[8]

§ 4. Discussion on calculated results

§ 4-1 *Density region of the $^3P_2$- and $^1S_0$-superfluid state*

From Fig. 2 we can conclude that there exists a $^3P_2$-superfluid state in the density region $\rho \simeq (2\sim8)\times10^{14}$gcm^{-3} and that the effect of the $^3P_2$-$^3F_2$ tensor coupling plays a role indispensable to the existence of the $^3P_2$-superfluid state in neutron-star matter. We have the maximum value of the energy gap, $\Delta_{10}^{\lambda}(k_F)$ at $\rho \simeq 4\times10^{14}$gcm^{-3} ($E_F=76$ MeV) and its value is about 0.6 MeV. As ρ goes away from the above value, $\Delta_{10}^{\lambda}(k_F)$ is seen to decrease quite rapidly. For the low-density side ($\rho \simeq (2\sim3.5)\times10^{14}$gcm^{-3}, $E_F \simeq (50\sim70)$MeV), which is mainly due

to that the two-nucleon attractive potentials are masked by the centrifugal effect. For the high-density one ($\rho\simeq(5\sim8)\times10^{14}\mathrm{gcm}^{-3}$, $E_F\simeq(90\sim120)\mathrm{MeV}$), which is mainly caused by the fact that m^* becomes smaller as ρ increases. But the above results for higher densities ($\rho\gtrsim6\times10^{14}\mathrm{gcm}^{-3}$) get quantitatively somewhat less reliable than for lower densities, because the applicability of Brueckner theory up to such a high density is an open question.[6]

The $^1S_0$-superfluid state is seen to exist in the region $\rho\simeq(1.0\times10^{11}\sim1.5\times10^{14})\mathrm{gcm}^{-3}$. On the basis of these results, the neutron-star matter in the region $\rho\simeq(1.5\sim2.0)\times10^{14}\mathrm{gcm}^{-3}$ is considered to be normal. In our calculation, the density at which the $^1S_0$-gap vanishes is somewhat higher than that calculated by Ishihara et al.,[10] R. Kennedy et al.[11] and N.-C. Chao et al.,[5] but is approximately equal to that calculated by M. Hoffberg et al.[4] The small differences may be due to the variety in the calculational methods, the potentials and the m^* values adopted. Therefore, we cannot deny a possibility that the density region of the $^1S_0$-superfluid state becomes somewhat narrower in the high-density side and the density region of the normal state in neutron-star matter is wider than that concluded above. In the neutron star, a gas of free neutrons appears at $\rho\simeq3\times10^{11}\mathrm{gcm}^{-3}$ [12),13)] therefore our results suggest that the free neutrons are in the superfluid state as soon as they appear in the neutron star.

§ 4-2 *The influence of the tensor coupling on the total energy shift*

The total energy shift is estimated by the relation[3]

$$\Delta E\simeq-N_F\int d\hat{k}D_\lambda^2(k_F,\hat{k})/8\pi\,, \tag{4·1}$$

where $N_F=3N/4E_F$ is the level density at $k=k_F$ for the total neutron number N and the explicit form for the solution with and without the tensor coupling in the case of $m_j=0$ component only is

$$\Delta E_{m_j=0}^{\text{couple}}\simeq-N_F/16\pi\cdot\{(\Delta_{10}^{\lambda}(k_F))^2+(\Delta_{30}^{\lambda}(k_F))^2\} \tag{4·2}$$

and

$$\Delta E_{m_j=0}^{\text{uncouple}}\simeq-N_F/16\pi\cdot(\Delta_{10}^{\prime\lambda}(k_F))^2, \tag{4·3}$$

respectively, where $\Delta_{10}^{\prime\lambda}(k_F)$ is the $^3P_2$-gap without the tensor coupling. Equation (4·2) shows that not only the $^3P_2$-gap but also the $^3F_2$-gap contribute to the total energy shift due to the $^3P_2$-$^3F_2$ tensor coupling. For $m^*=1$ and $E_F=100\,\mathrm{MeV}$, the ratio $(\Delta_{10}^{\lambda}(k_F)/\Delta_{10}^{\prime\lambda}(k_F))^2$ takes the value of ~2.3 and $(\Delta_{30}^{\lambda}(k_F)/\Delta_{10}^{\lambda}(k_F))^2\sim0.03$, as is seen from Fig. 5. From these we can say that the contribution of $\Delta_{30}^{\lambda}(k_F)$ to $\Delta E_{m_j=0}^{\text{couple}}$ is negligibly small compared with that of $\Delta_{10}^{\lambda}(k_F)$ and the increase of the total energy shift due to the effect of the $^3P_2$-$^3F_2$ tensor coupling is caused wholly by the increase of the $^3P_2$-gap due to this effect. The total energy shift becomes large by a factor ~2.3 by this effect.

§ 4-3 *Remarks on the state of the interior of a neutron star*

Density distribution in the interior of a neutron star is strongly connected with its mass M. As is already mentioned, the existence of the superfluid state in neutron-star matter strongly depends on its density. In connection with these, it is interesting to investigate how the state of the interior of neutron stars is connected with their masses. At this stage, we can use our results that neutrons in neutron stars are in the $^3P_2$-superfluid state for $\rho \simeq (2 \sim 8) \times 10^{14} \mathrm{gcm}^{-3}$, in the $^1S_0$-superfluid one for $\rho \simeq (1.0 \times 10^{11} \sim 1.5 \times 10^{14}) \mathrm{gcm}^{-3}$ and in the normal state for $\rho \simeq (1.5 \sim 2.0) \times 10^{14} \mathrm{gcm}^{-3}$. The proton density in a neutron star is so low that protons are considered to be in the $^1S_0$-superfluid state.[3),5)] Here we discuss only the states of the neutrons in a neutron star. Making use of the above mentioned results and the density distribution as a function of the distance r from the center of a neutron star, we can see what portion of a neutron star is occupied by the normal fluid or the superfluid. This is shown in Fig. 9 with the aid of the recent results of the neutron-star model obtained by Ikeuchi et al.[6)] for $M/M_\odot = 0.55$, where $M_\odot$ denote the solar mass. In this case, the $^3P_2$-superfluid occupies the region of $r \simeq (4.0 \sim$

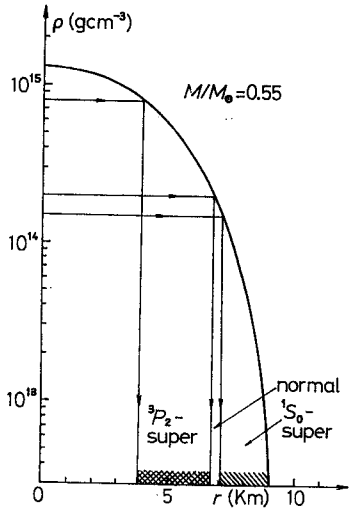

Fig. 9. ρ-r (the distance from the center of a neutron star) curve obtained by Ikeuchi et al. for $M/M_\odot = 0.55$ and the procedure to know the state of the interior of a neutron star.

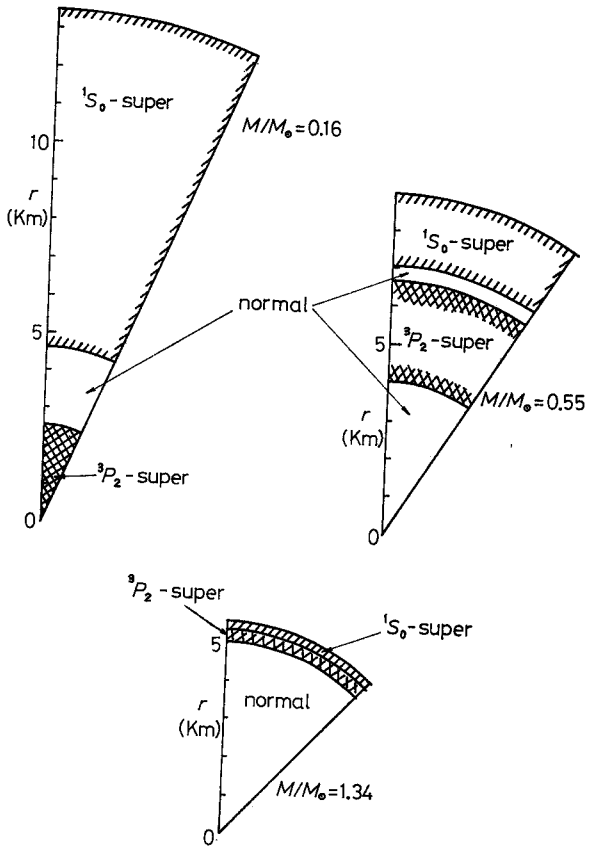

Fig. 10. Mass-dependence of the multiphase structure of the interior of neutron stars.

6.7) km and the $^1S_0$-superfluid occupies that of $r\simeq(7.1\sim9.0)$km. The regions of $r\simeq(6.7\sim7.1)$km and $r\lesssim4$ km are in the normal state. In this way, we can know the state of the interior of a neutron star. For other typical masses of neutron stars, $M=0.16M_\odot$ and $M=1.34M_\odot$, the same procedure is used to draw the schematic graphs in Fig. 10, representing how the structure of the interior of neutron stars changes according to their masses.

These graphs show that as M becomes large, each of the layers, where the $^1S_0$- and $^3P_2$-superfluids occupy, becomes thinner and shifts to the outer side, while as M becomes small it becomes thicker and expands to the inner side. The layer of the normal state existing between the $^1S_0$-superfluid layer and the $^3P_2$-one has a tendency that it expands as M becomes small. For a neutron star with small mass such as $M/M_\odot\lesssim0.16$, the superfluids occupy a large portion of it and the $^3P_2$-superfluid fills particularly its core region. On the other hand, for a neutron star with a large mass such as $M/M_\odot\gtrsim1.34$, the normal fluid occupies a wide region extending from its core region to its surface. Based on these results, we want to remark the following points: The structure of the interior of a neutron star strongly depends on the mass. Therefore we must pay attention to the strong-density dependence of existence of the energy gaps when we discuss the properties of neutron stars connected with the superfluidity. The multiphase structure of the interior of a neutron star is dependent on neutron star models. For example, the $^3P_2$-superfluid expands to a core region of a neutron star for a model shown by Cameron[12] for the case of $M/M_\odot\simeq0.55$, differing from the results shown in Fig. 10.

Acknowledgements

The author would like to express his sincere thanks to Professor R. Tamagaki for initiating the author into this series of investigation, useful advice and valuable discussions. The author wishes to thank Professor S. Nagata for making his results on one-body potential in neutron-star matter available to the author and is grateful to Professor Y. Katayama for his continuous encouragement.

Appendix A

——Proof of Eq. (2·14)——

If we impose the time-reversal invariance on the transformation operator S in Eq. (2·7), we can derive the following condition on $\theta_\lambda(\boldsymbol{k}\sigma_1\sigma_2)$ given in Eq. (2·9):

$$\theta_\lambda^*(-\boldsymbol{k},-\sigma_1,-\sigma_2)=(-)^{1+\sigma_1+\sigma_2}\theta_\lambda(\boldsymbol{k},\sigma_1,\sigma_2). \tag{A·1}$$

For the triplet case, because $s=1$ and $l=$odd, $\boldsymbol{\theta}_\lambda(\boldsymbol{k})$ is a symmetric matrix and odd for $\boldsymbol{k}\to-\boldsymbol{k}$. On the other hand, for the singlet case, $\boldsymbol{\theta}_\lambda(\boldsymbol{k})$ is an antisym-

metric matrix and even for $\boldsymbol{k}\to-\boldsymbol{k}$ because $s=0$ and $l=$even. By the use of Eq. (A·1) and the above mentioned properties of $\hat{\theta}_\lambda(\boldsymbol{k})$, the following relations are obtained:

$$\begin{cases}\theta_\lambda^*(\boldsymbol{k},\ -\sigma_1,\ -\sigma_2)=(-)^{\sigma_1+\sigma_2}\theta_\lambda(\boldsymbol{k},\sigma_1,\sigma_2),\\ \theta_\lambda(\boldsymbol{k},\sigma_1,\sigma_2)=\theta_\lambda(\boldsymbol{k},\sigma_2,\sigma_1)\end{cases}\tag{A·2}$$

for the triplet case and

$$\begin{cases}\theta_\lambda^*(\boldsymbol{k},\ -\sigma_1,\ -\sigma_2)=(-)^{1+\sigma_1+\sigma_2}\theta_\lambda(\boldsymbol{k},\sigma_1,\sigma_2),\\ \theta_\lambda(\boldsymbol{k},\sigma_1,\sigma_2)=-\theta_\lambda(\boldsymbol{k},\sigma_2,\sigma_1)\end{cases}\tag{A·3}$$

for the singlet case. In any case, we can easily show that $\hat{\theta}_\lambda'(\boldsymbol{k})$ given in Eq. (2·13) is written in the form proportional to unit matrix by using the relations given in Eqs. (A·2) and (A·3):

$$\hat{\theta}_\lambda(\boldsymbol{k})\equiv\begin{pmatrix}\theta_\lambda(\boldsymbol{k}\uparrow\uparrow) & \theta_\lambda(\boldsymbol{k}\uparrow\downarrow)\\ \theta_\lambda(\boldsymbol{k}\downarrow\uparrow) & \theta_\lambda(\boldsymbol{k}\downarrow\downarrow)\end{pmatrix},$$

$$\hat{\theta}_\lambda'(\boldsymbol{k})=\pm\theta_D(\boldsymbol{k})\begin{pmatrix}1 & 0\\ 0 & 1\end{pmatrix},\tag{A·4}$$

where

$$\theta_D(\boldsymbol{k})=\sqrt{|\theta_\lambda(\boldsymbol{k}\uparrow\uparrow)|^2+|\theta_\lambda(\boldsymbol{k}\uparrow\downarrow)|^2}\tag{A·5}$$

for the triplet case and

$$\theta_D(\boldsymbol{k})=|\theta_\lambda(\boldsymbol{k}\uparrow\downarrow)|\tag{A·6}$$

for the singlet case. Here we note that $\theta_D(\boldsymbol{k})$ is real and has the following relation:

$$\theta_D(\boldsymbol{k})=\theta_D(-\boldsymbol{k}).\tag{A·7}$$

In the partial wave representation, the condition given in Eq. (A·1) is equivalent to

$$\phi_{lm_j}^{*\lambda}(k)=(-)^{j+m_j}\phi_{l,-m_j}^{\lambda}(k).\tag{A·8}$$

By the use of Eq. (A·8), we obtain the following relation:

$$\Delta_{lm_j}^{*\lambda}(k)=(-)^{j+m_j}\Delta_{l,-m_j}^{\lambda}(k)\tag{A·9}$$

in the same form given in Appendix B in I even with the presence of the tensor coupling.

Appendix B

——General proof of Eqs. (3.13 a∼d) in I in the case with the tensor coupling——

As is mentioned in Appendix A, $\hat{\theta}_\lambda(\boldsymbol{k})$ has the properties

$$\tilde{\boldsymbol{\Phi}}_\lambda(-\boldsymbol{k}) = -\boldsymbol{\Phi}_\lambda(\boldsymbol{k}). \tag{B·1}$$

By the use of Eq. (A·4), we can rewrite $U_\lambda(\boldsymbol{k})$ and $V_\lambda(\boldsymbol{k})$ in the following form:

$$U_\lambda(\boldsymbol{k}) = \cos \boldsymbol{\Phi}_\lambda'(\boldsymbol{k}) = \begin{pmatrix} u_{\boldsymbol{k}} & 0 \\ 0 & u_{\boldsymbol{k}} \end{pmatrix}, \tag{B·2}$$

$$\begin{aligned} V_\lambda(\boldsymbol{k}) &= \boldsymbol{\Phi}_\lambda'^{-1}(\boldsymbol{k}) \sin \boldsymbol{\Phi}_\lambda'(\boldsymbol{k}) \boldsymbol{\Phi}_\lambda(\boldsymbol{k}) \\ &= \begin{pmatrix} v_{\boldsymbol{k}} & 0 \\ 0 & v_{\boldsymbol{k}} \end{pmatrix} \boldsymbol{\Phi}_\lambda(\boldsymbol{k}), \end{aligned} \tag{B·3}$$

where

$$u_{\boldsymbol{k}} = \cos \theta_D(\boldsymbol{k}) \tag{B·4}$$

and

$$v_{\boldsymbol{k}} = \sin \theta_D(\boldsymbol{k}) / \theta_D(\boldsymbol{k}). \tag{B·5}$$

By the use of Eqs. (B·1∼5) and Eq. (A·7) with $\theta_D(\boldsymbol{k})$ being real, we can easily verify that Eqs. (3·13a∼d) in I holds for the case with the tensor coupling.

References

1) T. Takatsuka, Prog. Theor. Phys. Letters **47** (1972), 1062.
2) R. Tamagaki, Prog. Theor. Phys. **44** (1970), 905.
3) T. Takatsuka and R. Tamagaki, Prog. Theor. Phys. **46** (1971), 114.
4) M. Hoffberg, A. E. Glassgold, R. W. Richardson and M. Ruderman, Phys. Rev. Letters **24** (1970), 775.
5) N. -C. Chao, J. W. Clark and C. -H. Yang, Nucl. Phys. **A179** (1972), 320.
6) S. Ikeuchi, S. Nagata, T. Mizutani and K. Nakazawa, Prog. Theor. Phys. **46** (1971), 95.
7) R. Tamagaki, Prog. Theor. Phys. **39** (1968), 91.
8) T. R. Mongan, Phys. Rev. **178** (1969), 1597.
9) F. Tabakin, Ann. of Phys. **30** (1964), 51.
10) T. Ishihara, R. Tamagaki, H. Tanaka and M. Yasuno, Prog. Theor. Phys. **30** (1963), 601.
11) R. Kennedy, L. Wilets and E. M. Henley, Phys. Rev. **133** (1964), B1131.
12) A. G. W. Cameron, Ann. Rev. Astron. Astrophys. **8** (1970), 179.
13) H. A. Bethe, G. Börner and K. Sato, Astron. & Astrophys. **7** (1970), 279.